Check for updates

View Article Online
View Journal

PCCP
Physical Chemistry Chemical Physics

Accepted Manuscript

This article can be cited before page numbers have been issued, to do this please use: M. Idrees, C. Nguyen, B. H, I. Ahmad and B. Amin, *Phys. Chem. Chem. Phys.*, 2020, DOI: 10.1039/D0CP03434G.

This is an Accepted Manuscript, which has been through the Royal Society of Chemistry peer review process and has been accepted for publication.

Accepted Manuscripts are published online shortly after acceptance, before technical editing, formatting and proof reading. Using this free service, authors can make their results available to the community, in citable form, before we publish the edited article. We will replace this Accepted Manuscript with the edited and formatted Advance Article as soon as it is available.

You can find more information about Accepted Manuscripts in the Information for Authors.

Please note that technical editing may introduce minor changes to the text and/or graphics, which may alter content. The journal's standard Terms & Conditions and the Ethical guidelines still apply. In no event shall the Royal Society of Chemistry be held responsible for any errors or omissions in this Accepted Manuscript or any consequences arising from the use of any information it contains.

ROYAL SOCIETY OF CHEMISTRY

rsc.li/pccp

View Article Online
DOI: 10.1039/D0CP03434G

ROYAL SOCIETY OF CHEMISTRY

Journal Name

ARTICLE TYPE

Cite this: DOI: 10.1039/xxxxxxxxxx

Van der Waals heterostructures based on MSSe (M = Mo, W) and graphene-like GaN: Enhanced optoelectronic and photocatalytic properties for water splitting

M. Idrees[1], Chuong V. Nguyen[2†], H. D. Bui[3†], Iftikhar Ahmad[4], Bin Amin[5†]

Received Date
Accepted Date

DOI: 10.1039/xxxxxxxxxx

www.rsc.org/journalname

The geometric structure, electronic, optical and photocatalytic properties of MSSe-g-GaN (M = Mo, W) van der Waals (vdW) heterostructures are investigated by performing first-principles calculations. We find that the MoSSe-g-GaN heterostructure exhibits type-II band alignment for all stacking patterns. While the WSSe-g-GaN heterostructure forms the type-II or type-I band alignment for the stacking model-I or model II, respectively. The average electrostatic potential shows that the potential of g-GaN is deeper than the MSSe monolayer, leading to the formation of electrostatic field across the interface, causing the transfer of photogenrated electrons and holes. Efficient interfacial formation of interface and charge transfer reduce the work function of MSSe-g-GaN vdW heterostructures as compared to the constituent monolayer. The difference in the carrier mobility for electron and hole suggests that these heterostructures could be utilized for hole/electron separation. Absorption spectra demonstrate that strong absorption from infrared to visible light in these vdW heterostructures can be achieved. Appropriate valence and conduction band edges positions with standard redox potentials provide enough force to drive the phototgenerated electrons and holes to dissociate water into H^+/H_2 and O_2/H_2O at pH = 0.

1 Introduction

Recently, a new class of intriguing two-dimensional (2D) materials with general formula MXY (M = Mo,W; X/Y = S, Se, Te), namely Janus monolayers, has been successfully synthesized by chemical vapor deposition of Se in MoS_2 [1] and S in $MoSe_2$ [2]. Furthermore, using density functional theory (DFT), Zhang et al.[2] proved that the electronic structures and Raman vibration modes of Janus MoSSe monolayer are found to correlate well with experimental measurements. Using DFT calculations, Tao et al.[3] demonstrated that the electronic properties, Zeeman-type spin splitting and valley polarization of Janus MXY monolayers are found to be well preserved like their parent (MX_2) phases. Moreover, a Rashba spin splitting around the Γ-point was also observed in these Janus monolayers, making them promising candidates for future spintronics. Xia et. al.[4] showed that the induced dipole moment, vibrational frequency, Rashba parameters, and direct to indirect band gap transition in Janus MXY (M = Mo, W; X/Y = S, Se, Te) monolayers are associated with the atomic radius and electronegativity differences of the chalcogen X/Y atoms.

Similar to the parent (MX_2) phases[5–7], the high recombination ratio and short life time of photogenrated electron-hole pairs in Janus MXY monolayers would also hinder their practical applications. To control this issue and further tune the properties of the 2D materials, layer stacking in the form of van der Waals (vdW) heterostructures is used intensively for designing viable electronic products[8–12]. In vdW heterostructure with type-II band alignment[13], both the valence band maximum (VBM) and conduction band minimum (CBM) of one layer are lower than the corresponding VBM and CBM of the other one, hence, electrons and holes migrate from one layer to the other. Therefore, the unwanted combination of photogenerated carriers is avoided, which significantly increases their life time[14].

Very recently, Idrees et al.[15] theoretically predicted that Janus vdW heterostuctures of MoSSe-WSSe, MoSeTe-WSeTe and MoSTe-WSTe are indirect band gap semiconductors with type-II band alignment. In addition, they found that the external electric field and tensile strain can transform some of the above mentioned vdW heterostructures from an indirect to a direct band gap. A strong device absorption efficiency of about 80-90 % is observed for Janus WSeTe, MoSTe and WSTe monolayers in the

[1] Department of Physics, Hazara University, Mansehra 21300, Pakistan
[2] Department of Materials Science and Engineering, Le Quy Don Technical University, Ha Noi 100000, Viet Nam: Email: chuongnguyen11@gmail.com
[3] Institute of Research and Development, Duy Tan University, Da Nang 550000, Vietnam: Email: buidinhhoi@duytan.edu.vn
[4] Department of Physics, University of Malakand, Chakdara, 18800, Pakistan
[5] Department of Physics, Abbottabad Uniersity of Science and Technology, Abbottabad 22010, Pakistan. Email: binukhn@gmail.com
† To whom correspondence should be addressed. Email: chuongnguyen11@gmail.com; buidinhhoi@duytan.edu.vn; binukhn@gmail.com

Published on 21 August 2020. Downloaded by University of Vermont on 8/23/2020 5:51:36 PM.

Physical Chemistry Chemical Physics Accepted Manuscript

View Article Online
DOI: 10.1039/D0CP03434G

Published on 21 August 2020. Downloaded by University of Vermont on 8/23/2020 5:51:36 PM.

visible, infrared and ultraviolet regions, whereas energetically favorable band edge positions make the MoSSe-WSSe heterostructure a promising candidate for water splitting. Recently, a direct type-II band alignment and considerable Rashba spin splitting in GeC-MSSe (M = Mo, W) vdW heterostructures have shown to provide a platform for experimental and theoretical understanding of spintronic devices based on 2D materials [16]. More interestingly, appropriate band alignments with the standard water redox potentials enable of these heterostructures to dissociate water into H^+/H_2 and O_2/H_2O.

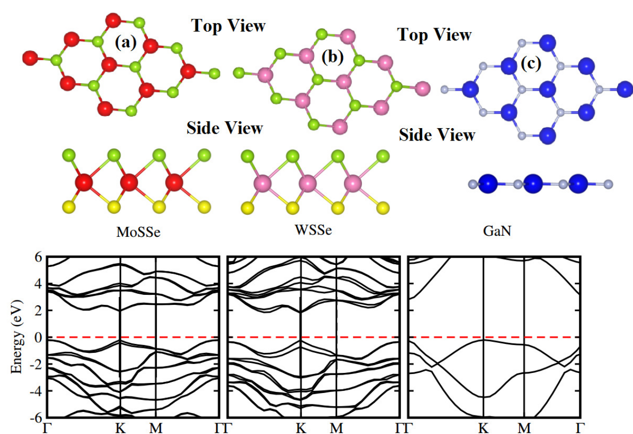

Fig. 1 Top view (first row), side view (second row) and electronic band structure (third row) of (a) isolated MoSSe, (b) WSSe and (c) g-GaN monolayers. Red, cyan, yellow and green balls stand for Mo, W, S and Se atoms, respectively. Dark blue and light blue balls represent the Ga and N atoms, respectively.

Currently, graphene-like gallium nitride (g-GaN) has been successfully fabricated through migration-enhanced encapsulated-growth [17]. The g-GaN monolayer has a band gap band gap of 2.158/4.0 eV calculated using DFT/G_0W_0 method [18,19]. The electronic properties of g-GaN can further be modified by adsorption, doping and elastic strain [20] and van der Waals heterostructures [21–23]. Among these, the formation of van der Waals heterostructures by combining different 2D materials has been proved to be one of the most effective approaches to modify and enhance electronic, optical properties and photocatalytic performance of GaN monolayer. For instance, Sun and his co-authors [21] demonstrated that the type-II vdW heterostructure of g-GaN and Blue phosphorene (BlueP) suggests a promising application as a photocatalyst. Wang et al. [22] demonstrated that integrating two-dimensional MoS_2 on GaN surface into vdW heterostructures can create the possibility to induce novel electronic and optical properties of GaN monolayer. All these studies predicted that the formation of vdW heterostructures between GaN and other 2D materials exhibit excellent electronic and optoelectronic properties and great potential in optoelectronics and photovoltaics.

Therefore, in this paper, we present the unusual properties of MSSe-g-GaN (M = Mo, W) vdW heterostructures using DFT calculations in the Vienna Ab-initio Simulation Package [24–28]. Furthermore, Ab-initio molecular dynamics (AMD) [29,30] simulations are used to check the thermal stability of these systems. Two different models with alternative chalcogen atoms having four

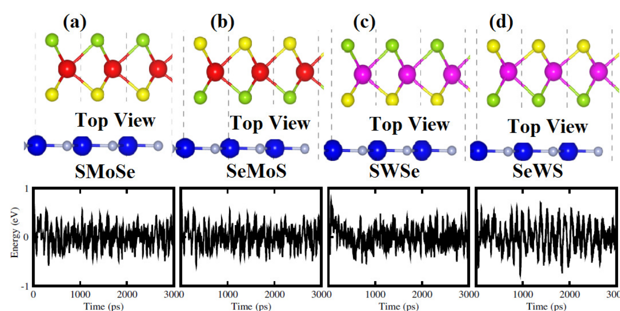

Fig. 2 Top views (first row) and thermal stability (second row) of the most energetically favorable stacking configurations of MoSSe-g-GaN heterostructures for (a) model-I, (b) model-II, and WSSe-g-GaN (c) model-I, (d) model-II.

possible stacking configurations of vdW heterostructures are constructed. Our study reveals that all the MSSe-g-GaN vdW heterostructures for both models are energetically stable and are direct band gap semiconductors with type-II band alignment. Furthermore, Bader charge analysis, planer and average electrostatic potentials, carrier transfer capacity, work function, optical and photocatalytic response of all these materials are also investigated. Our finding suggests that MSSe-g-GaN (M = Mo, W) vdW heterostructures could be potential candidate for optoelectronic, photovoltaic and photocatalysis devices.

2 Computational details

All the structural relaxation and electronic properties calculations of the MSSe, GaN monolayers and their corresponding heterostructures are performed on the framework of DFT method using the Vienna Ab-initio Simulation Package [24–28] within the projector augmented wave (PAW) pseudopotentials. The generalized gradient approximation (GGA) with the Perdew-Burke-Ernzerhof (PBE) function is selected to describe the exchange and correlation energy. The traditional DFT-PBE method underestimates the band gap values of materials, especially semiconducting 2D materials, thus, we opt to use the hybrid functional HSE06 to overcome this issue. Furthermore, the weak interactions that always occur in the layered materials are described by using the Grimme DFT-D2 method. For plane wave basis we set a cutoff energy to 410 eV with the convergence of energy and force of 10^{-6} eV/Å and 10^{-4} eV, respectively. To eliminate unphysical interactions of materials, we use a large vacuum thickness of 25 Å along the z direction. A $9 \times 9 \times 1$ k-mesh is used to sample the first Brillouin zone integration.

The optical characteristics of the constituent monolayers and their heterostructures are calculated using the Bethe-Salpeter equation (BSE) on top of single-shot G_0W_0 calculations as follows:

$$\varepsilon_2(\omega) = \frac{4\pi^2 e^2}{\Omega} \lim_{q \to 0} \frac{1}{q^2} \sum_{c,v,k} 2\omega_k \delta(\varepsilon_{ck} - \varepsilon_{vk} - \omega) \times \langle u_{ck+e_{\alpha q}|u_{vk}} \rangle \times \langle u_{ck+e_{\alpha q}|u_{vk}} \rangle^* . \quad (1)$$

Physical Chemistry Chemical Physics Accepted Manuscript

This journal is © The Royal Society of Chemistry [year]

View Article Online
DOI: 10.1039/D0CP03434G

Table 1 Calculated elastic modulus (C_{2D}, N/m), deformation potential constant (E_1, eV), carrier effective mass (m^*/m_0) and carrier mobility (μ, cm^2/Vs)for electrons (e) and holes (h) of g-GaN, MSSe monolayers and their corresponding vdW heterostructures for different stacking types.

Material	C_{2D}	E_e^1	E_h^1	m_e^*	m_h^*	μ_e	μ_h
MoSSe	152	10.27	6.54	0.54	0.64	179.56	303.66
WSSe	68	13.42	1.01	0.21	1.19	299.66	1647.55
GaN	140	12	5.01	0.30	0.42	378.08	1106.68
Model-I							
MoSSe-g-GaN	110	8.34	1.13	0.34	1.18	480.30	2172.10
WSSe-g-GaN	104	10.24	0.91	0.27	1.15	477.65	3333.93
Model-II							
MoSe-g-GaN	109	8.73	1.10	0.31	1.16	520.88	2343.11
WSSe-g-GaN	103	9.34	3.21	0.28	0.38	528.33	2428.50

Where, c and v are the CBM and VBM of materials, respectively. u_{ck} presents the cell periodic part of wavefunctions.

3 Results and discussion

We first check the lattice parameters of MoSSe, WSSe and g-GaN monolayers, which are calculated to be 3.25 Å, 3.26 Å, and 3.25 Å. These results agree well with previous reports [15,16,31], indicating the reliability of our computational approach. Schematic top (side) view and band structures of MoSSe, WSSe and g-GaN monolayers are presented in Fig 1. One can observe from Fig. 1 that both MoSSe and WSSe monolayers exhibit direct band gap semiconduction with band gaps of 2.24 eV and 2.16 eV, respectively. Both the VBM and CBM of semiconducting MoSSe and WSSe monolayer are located at the K point. On the contrary, g-GaN is an indirect semiconductor with band gap of 3.2 eV, formed between the VBM at the K point and the CBM at the Γ point. All these results are in good agreement with previous reports [15,19,31].

Hexagonal MoSSe, WSSe and g-GaN monolayers as depicted in Fig. 1 display satisfying lattice mismatches, hence realizing the possible experimental fabrication of MSSe-g-GaN (M = Mo, W) vdW heterostructures for practical applications. In general, local configurations and specific contacted atoms significantly modulate the properties of vdW heterostructure, therefore, we considered four possible staking layers in two different models with alternate positions of S/Se atoms at opposite surfaces of MSSe in MSSe-g-GaN vdW heterostructures, as illustrated in Fig. 2. In Model-I, stacking (I), a Mo/W atom is placed on top of a N atom while a S/Se atom is on top of a Ga; stacking (II), a Mo/W atom is placed on top of a Ga atom while a S/Se atom is on top of a N atom; stacking (III), a Mo/W atom is placed on top of a Ga atom while a N atom is centered at the hexagonal ring; stacking (IV), a Mo/W atom is placed on top of a N atom while a Ga atom is centered at a hexagonal ring. All these stacking patterns of the MSSe-g-GaN heterostructures are illustrated in Fig. S1 of Supplementary Information. We have also relaxed all the similar stacking sequences in model-II as discussed. Favorable stacking patterns are obtained by means of the binding energy and interlayer distance.

The binding energy is given by [32,33], $E_b = E_{\text{MSSe-g-GaN}} - E_{\text{MSSe}} - E_{\text{g-GaN}}$, where $E_{\text{MSSe-g-GaN}}$ represents the total energy of the MSSe-g-GaN vdW heterostructure. E_{MSSe} and $E_{\text{g-GaN}}$ are the total energies of isolated MSSe (M = Mo, W) and g-GaN monolayers, respectively. Based on this definition, our calculated binding energy/interlayer distance of MoSSe-g-GaN (WSSe-g-GaN) for model-I and model-II is -0.48 eV/3.0 Å (-0.35 eV/2.95 Å) and -0.41 eV/3.02 Å (-0.32 eV/3.05 Å), respectively. In addition, both the interlayer distance and binding energy of the MSSe-g-GaN heterostructures for all stacking configurations are listed in Tab. S1 of Supplementary Information. One can find from Fig. S1 of Supplementary Information that the stacking IV configuration of the MSSe-g-GaN heterostructure has the shortest interlayer distance and the lowest binding energy as compared to other stacking configurations. These results suggest that stacking (IV) is the most favorable stacking configuration. Furthermore, these values are comparable with those in other vdW heterostructures [15,16], demonstrating that all these heterostructures are characterized by weak vdW forces. In addition, the thermal stability of these heterostructures is also confirmed by performing AIMD simulations

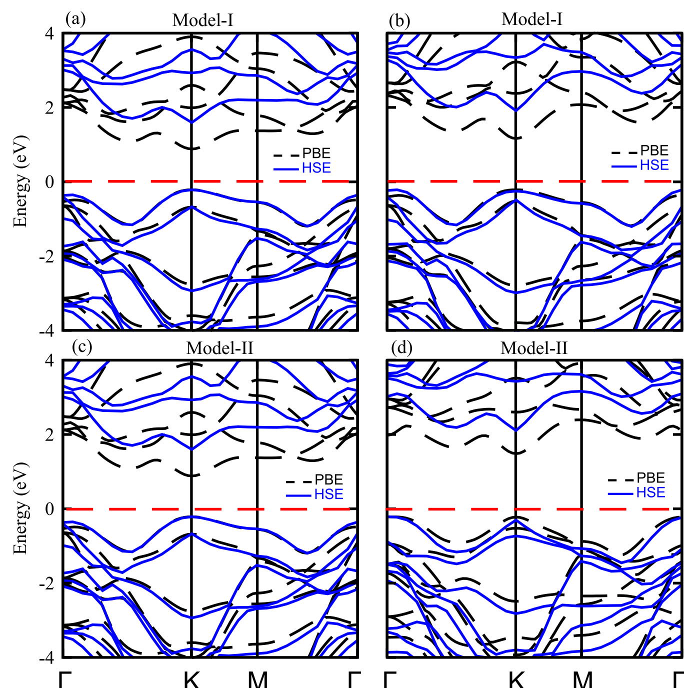

Fig. 3 Electronic band structures of MoSSe-g-GaN heterostructures for (a) model-I, (c) model-II and WSSe-g-GaN heterostructure for (b) model-I and (d) model-II.

Published on 21 August 2020. Downloaded by University of Vermont on 8/23/2020 5:51:36 PM.

Physical Chemistry Chemical Physics Accepted Manuscript

View Article Online
DOI: 10.1039/D0CP03434G

Published on 21 August 2020. Downloaded by University of Vermont on 8/23/2020 5:51:36 PM.

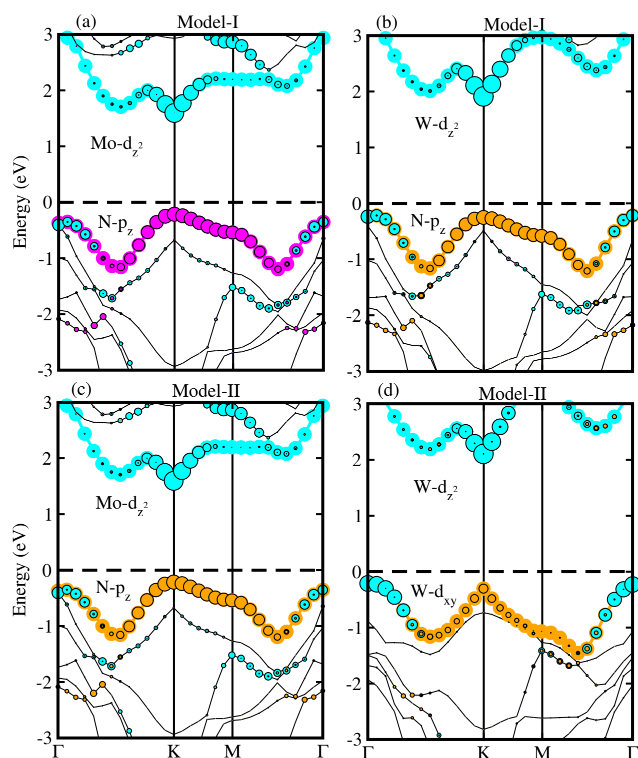

Fig. 4 HSE06 weighted band structure of MoSSe-g-GaN for (a) model-I, (c) model-II and WSSe-g-GaN for (b) model-I and (d) model-II.

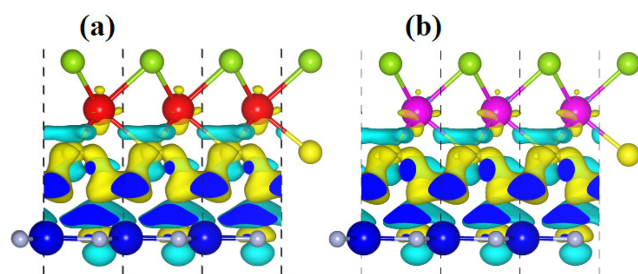

Fig. 5 Model-I, Charge density difference of (a) MoSSe-g-GaN and (b) WSSe-g-GaN vdW heterostructures.

through the Nose-thermostat algorithm at room temperature of 300 K for 3 ps. We find that MSSe-g-GaN vdW heterostructures retain their geometries without any structural distortion, as depicted in Fig. 2.

Using PBE[27] and HSE06[28] methods, the band structures of MSSe-g-GaN (M=Mo, W) vdW heterostructures in model-I and model-II are presented in Fig. 3. Interestingly, MSSe-g-GaN heterostructures in both model-I, and model-II have direct band gaps with VBM and CBM located at the K-point of BZ, while corresponding monolayer g-GaN(MSSe) is an indirect(direct) band gap semiconductor. The PBE band gap value in model-I/model-II of MoSSe-g-GaN is 1.07/1.05 eV and of WSSe-g-GaN is 1.36/1.71 eV, while HSE06 band gap value is 2.0/1.8 eV and 2.14/2.39 eV, respectively. It is obvious that a considerable difference is observed in the position of the CBM, while there is a minor difference in the position of the VBM. A similar trend was also observed in Janus MoSTe monolayer[34]. To gain deep insight into the

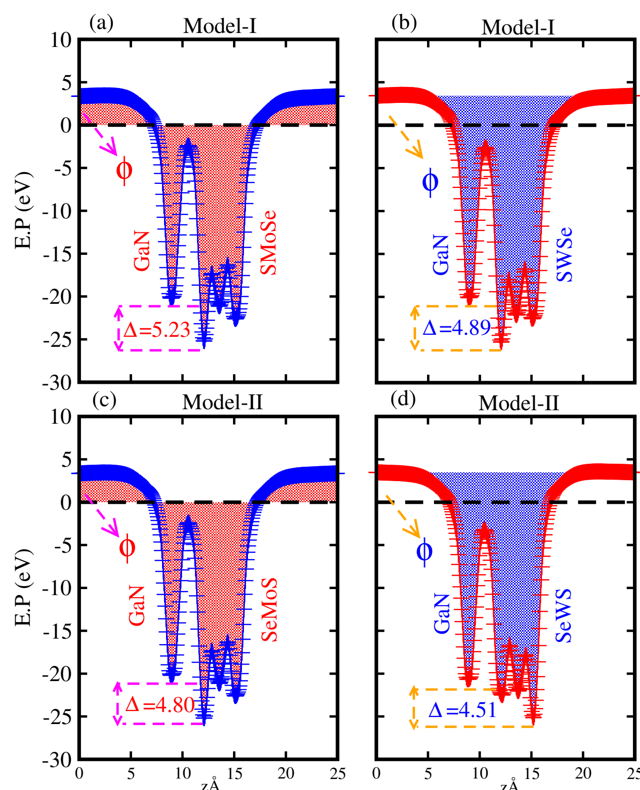

Fig. 6 Average electrostatic potential of MoSSe-g-GaN (a)model-I, (c) model-II and of WSSe-g-GaN (b)model-I, (d)model-II) vdW heterostructures. The potential drops and work functions are also presented.

band alignment, the weighted band structures of MSSe-g-GaN vdW heterostructures are calculated using the HSE06 method and presented in Fig. 4. It is obvious that the N-p_z orbital of the g-GaN monolayer contributes to the VBM, while the $Mo-d_{z^2}$ of MoSSe and $W-d_{z^2}$ of WSSe layers contribute to the CBM of MSSe-g-GaN vdW heterostructures for both stacking models. The $Mo(W)-d_{xy}$, $Mo(W)-d_{yz}$ and $Mo(W)-d_{xz}$ orbitals not participate to the band edges of heterostructures due to the strong coupling with $Ga-p$ orbitals, hence generating a significant split at bonding and anti-bonding states. The contributions from different layers to VBM and CBM of MSSe-g-GaN vdW heterostructure for both models confirm the formation of the type-II band alignment, which is similar to the MoS_2/SnO_2[35], CP/SiN and CAs/GeN heterostructures[36]. Effectively separated photogenerated carriers in type-II heterostructures indicate prominent applications of these vdW heterostructures in solar energy conversion, light emitting diodes and laser devices[37–39]. Furthermore, one can observe from Fig. 4(b) that the WSSe-g-GaN heterostructure for model-I exhibits type-II band alignment. The CBM of WSSe-g-GaN for the model-I comes from WSSe layer, whereas its VBM comes from g-GaN layer, confirming the formation of type-II band alignment. Whereas, the model-II of the WSSe-g-GaN heterostructure shows the type-I band alignment, as illustrated in Fig. 4(d). Both the CBM and VBM of such stacking configuration come from the WSSe layer, thus demonstrating the type-I band alignment.

Charge density differences (CDD) are investigated to get a qualitative understanding of the charge transfer in the MSSe-g-GaN

Physical Chemistry Chemical Physics Accepted Manuscript

This journal is © The Royal Society of Chemistry [year]

View Article Online
DOI: 10.1039/D0CP03434G

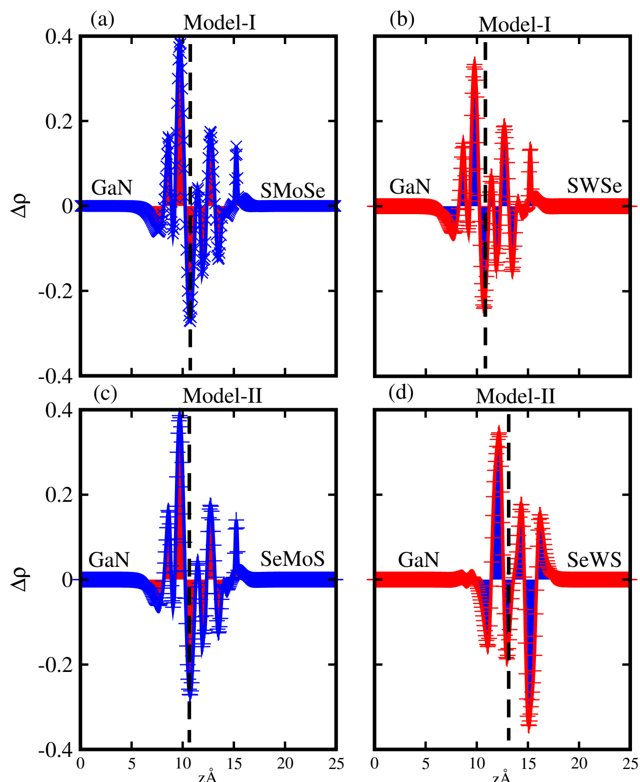

Fig. 7 Planer-averaged charge density difference of MoSSe-g-GaN (a)model-I, (c) model-II, and WSSe-g-GaN (b)model-I, (d)model-II) vdW heterostructures.

vdW heterostructures, as depicted in Fig. 5. The CDD is obtained by: $\Delta\rho = \rho_{\text{MSSe-g-GaN}}$ - ρ_{MSSe} - $\rho_{\text{g-GaN}}$, where $\rho_{\text{MSSe-g-GaN}}$, ρ_{MSSe} and $\rho_{\text{g-GaN}}$ represent the charge densities of heterostructures, isolated MSSe and g-GaN monolayers, respectively. One can observe from Fig. 5 that the g-GaN layer donates electrons to MSSe (M = Mo, W) layers for both models, resulting in the formation of *p*-doping type in g-GaN monolayer and *n*-doping type in Janus monolayers. Bader charge analysis[40] shows that for model-I (model-II) about 0.017 (0.015) electrons are transferred from the g-GaN layer to the MoSSe layer in the MoSSe-g-GaN heterostructure, while 0.023 (0.019) electrons are transferred from the g-GaN layer to the WSSe layer in the WSSe-g-GaN heterostructure. These values are comparable with those of our previous vdW heterostructures[15,16].

Consequently, the excitonic behavior of MSSe-g-GaN vdW heterostructures can be quite different from that of the isolated MSSe and g-GaN layer, as the gradient of the potential across the interface may facilitate the separation of electrons and holes[41]. The average electrostatic potential shows that the g-GaN layer has a deeper potential than the MSSe monolayers, as illustrated in Fig. 6, forming an electrostatic field across the interface and leading to the charge transfer from g-GaN to Janus monolayers. The potential drops between MoSSe (WSSe) and g-GaN layers are found to be 5.23 (4.80) eV for MoSSe-g-GaN and 4.89 (4.51) eV for WSSe-g-GaN, respectively, for model-I (model-II). These values show strong potential drops in MSSe-g-GaN vdW heterostructures, leading to a strong electrostatic field across the heterojunction, which has an effect on the transfer of photogenrated electrons and holes. It will also makes the difference in exitionic behavior between MSSe-g-GaN vdW heterostructure and the constituent MSSe and g-GaN monolayers. These findings help to facilitates electron and hole separation across the interface[42].

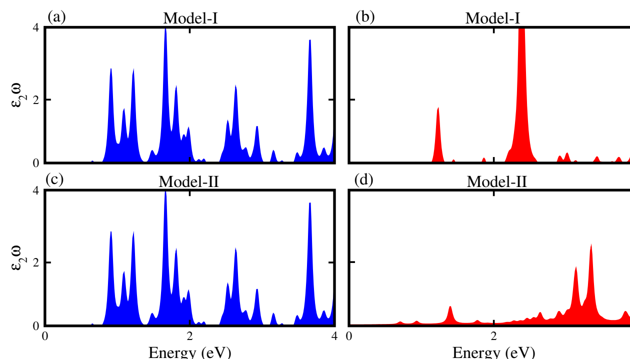

Fig. 8 Imaginary part of dielectric functions of MoSSe-g-GaN (a)model-I, (c)model-II, of WSSe-g-GaN (b) model-I, (d)model-II) vdW heterostructures

The transfers of electrons are also confirmed by the planar electrostatic potential, calculated by integrating the in-plane CDD from the formula $\Delta\rho(z) = \int \rho_{\text{Hetero}}(x,y,z)dxdy - \int \rho_{\text{MSSe}}(x,y,z)dxdy - \int \rho_{\text{g-GaN}}(x,y,z)dxdy$, as illustrated in Fig. 7. In this equation, $\rho_{\text{Hetero}}(x,y,z)$ is the charge density at the point (x,y,z) in the MSSe-g-GaN vdW heterostructures, $\rho_{\text{MSSe}}(x,y,z)$ represents the charge density at the point (x,y,z) in the MSSe monolayer, and $\rho_{\text{g-GaN}}(x,y,z)$ represents the charge density at the point (x,y,z) in the g-GaN monolayer. The amount of charge transfers along the z direction is calculated by $\Delta Q(z) = \int_{-\infty}^{z} \Delta\rho(z')dz'$. It is clear from Fig. 7 that the g-GaN layer donates electrons to the MSSe layers, making the g-GaN p-doping, while the MSSe monolayer n-doping.

Furthermore, it is interesting that the energy required to remove an electron from the Fermi level is the work function Φ, which can affect the properties of materials and improve the performance in solar cells. Φ can easily have an effect on the surface condition of a material, hence altering the surface electric field induced by the distribution of electrons at the interface[43]. The calculated values of Φ along the z direction[44] are 1.45 (1.29) eV for MoSSe-g-GaN and 1.56 (1.52) eV for WSSe-g-GaN vdW heterostructures for model-I (model-II). Moreover, the work function of MSSe-g-GaN vdW heterostructures is smaller than that of the constituent MSSe and g-GaN monolayers. The nature of such a decrease is due to the efficient interfacial formation and charge transfer[15,45,46]. In addition, we find that the work function of g-GaN is higher than that of MSSe monolayers, hence MSSe will be negatively charged, while g-GaN will be positively charged due to the high electrostatic induction which enhances the power conversion efficiency.

Using deformation potential (DP) theory, the carrier mobility (μ) of MSSe, g-GaN monolayers and MSSe-g-GaN vdW heterostructures is calculated[47]: $\mu_{2D} = e\hbar^3 C_{2D}/\kappa_B T|m^*|E_1^2$, where e is the electron charge, $\hbar$ is the reduced Planck constant, κ_B is Boltzmann's constant, T is the room temperature of 300 K, m^*

Physical Chemistry Chemical Physics Accepted Manuscript
Published on 21 August 2020. Downloaded by University of Vermont on 8/23/2020 5:51:36 PM.

View Article Online
DOI: 10.1039/D0CP03434G

Published on 21 August 2020. Downloaded by University of Vermont on 8/23/2020 5:51:36 PM.

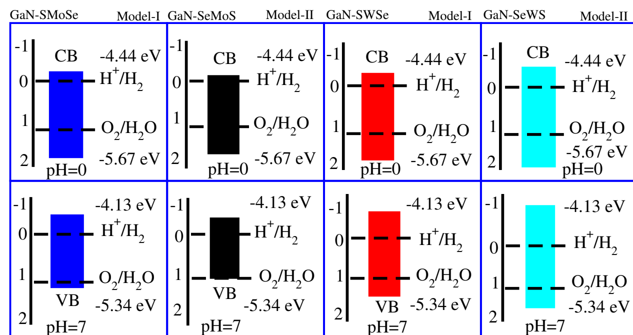

Fig. 9 Valence band (VB) and conduction band (CB) edge alignment of MSSe-g-GaN (M=Mo, W) vdW heterostructures, related to the vacuum level and standard redox potentials for water splitting at pH=0 and 7.

is the effective mass, E_1 is the deformation potential constant and C_{2D} is the in-plane stiffness. Electron and hole effective masses of MSSe, g-GaN monolayers and MSSe-g-Gan vdW heterostructures are calculated by $m^* = \hbar^2(\partial^2 E(k)/\partial k^2)^{-1}$. Interestingly, the effective mass of electrons is much smaller than that of holes, as listed in Table 1, indicating the easy drift of electrons towards holes. The in-plane stiffness (C_{2D}) of MSSe, g-GaN monolayers and MSSe-g-GaN vdW heterostructures is calculated by: $C_{2D} = [\partial^2 E/\partial \delta^2]/S_0$, where S_0 is the surface area of MSSe, gGaN monolayers and MSSe-g-GaN vdW heterostructures, respectively. The high carrier mobility of MSSe, g-GaN monolayers and MSSe-g-GaN vdW heterostructures demonstrates that these monolayers and vdW heterostructures have promising prospects in optoelectronic devices [48–51]. The difference in the carrier mobility of electrons and holes suggests that these heterostructures can be utilized for hole/electron separation [11].

We further calculate the imaginary part of the dielectric function ($\varepsilon_2(\omega)$) of MSSe-g-GaN vdW heterostructures by solving the Bethe-Salpeter equation, as depicted in Fig. 8. It is obvious that the optical transitions are dominated by excitons. In model-I, excitonic peaks are observed in the range of 1.70 eV (729 nm) for MoSSe-g-GaN, and at 1.50 eV (826 nm) for WSSe-g-GaN vdW heterostructures, while in model-II these peaks are observed at 1.78 eV (695 nm) for MoSSe-g-GaN, and at 1.56 eV (794 nm) for WSSe-g-GaN vdW heterostructures. The difference in the positions of these peaks with respect to Ref. [15,16] is due to the stacking of g-GaN with MSSe. Moreover, Fig. 8 also shows a systematic blue shift in the position of the excitonic peaks by changing a Mo atom with a W atom in the corresponding models. Exciton binding energies in model-I (model-II) are 0.40 (0.32) eV for MoSSe-g-GaN and 0.70 (0.64) eV for WSSe-g-GaN vdW heterostructure. It is also clear that the excitonic peaks are followed by the optical transition in the visible range, revealing a use for designing efficient optoelectronic devices [52–54] and photocatalysts [41].

The reduction/oxidation ability could be evaluated by the valence band (VB) and conduction band (CB) edges with respect to the water redox potential levels. Using the Mulliken electronegativity [55,56], the valence band is calculated by: $E_{\mathrm{VBM}} = \chi - E_{\mathrm{elec}} + 0.5E_{\mathrm{g}}$ and the conduction band: $E_{\mathrm{CBM}} = E_{\mathrm{VBM}} - E_{\mathrm{g}}$ at pH = 0 and pH = 7. These results are depicted in Fig. 9. E_{VBM} and E_{CBM} are the valence and conduction band edge potentials, χ represents the geometric mean of the Mulliken electronegativity of MSSe and g-GaN atoms and E_{elec} is the standard electrode potential on hydrogen scale with value of -4.5 eV, E_g is the calculated band gap. χ can be calculated by the geometric mean of electron affinity and first ionization potential of the corresponding atoms in MSSe and g-GaN monolayers. For pH = 7, we used the Nernst equation [57–59]: $E_{\mathrm{pH}} = E_{\mathrm{pH}=0} - 0.059 \times pH$, where $E_{pH} = 0$ is the value of the redox potential at pH = 0 and pH is the value of the redox potential.

The higher positions of VB and CB compared to those in standard redox potentials provides enough force to drive the photogenerated electrons and holes to dissociate water into H^+/H_2 and O_2/H_2O, thus making MSSe-g-GaN vdW heterostructures promising for water splitting at pH = 0. For pH = 7, all MSSe-g-GaN vdW heterostructures show a good response for photocatalytic water splitting, except for MoSSe-g-GaN in Model-II, which fails to reduced water to O_2. We predict that MSSe-g-GaN vdW heterostructures for both models at pH = 0 are good for photocatalytic water splitting, suggesting they are promising for low-cost and large-scale production of solar hydrogen. Similar results are also demonstrated for SiC-TMDCs, TMDCs-TMDCs and GeC-MSSe vdW heterostructures [15,16].

4 Conclusion

In summary, we have used DFT calculations to investigate the structural, electronic, optical, and photocatalytic properties of MSSe-g-GaN (M = Mo, W) vdW heterostructures. Stacking orders of minimal energy have been determined in model-I and model-II of MSSe-g-GaN heterostructures, which show direct band gaps with type-II band alignment. The charge density difference and Bader charge show that for model-I (model-II) about 0.017 (0.015) electrons are transferred from the g-GaN layer to the MoSSe layer, while 0.023 (0.019) electrons are transferred from the g-GaN layer to the WSSe layer. The average electrostatic potential shows that g-GaN layer has a deeper potential than the MSSe monolayers, raising a strong electrostatic field across the interface, leading to the transfer of photogenrated electrons and holes. Efficient interfacial formation of interface and charge transfer reduce the work function of MSSe-g-GaN vdW heterostructures. Hole and electron carrier mobility differences suggest that these heterostructures can be utilized for hole/electron separation. High carrier mobility in MSSe, g-GaN monolayers and MSSe-g-GaN vdW heterostructures demonstrates that these monolayers and heterostructures are promising for nanoelectronic and optoelectronic devices. Absorption spectra show that optical absorption is dominated by excitons, while strong absorption from infrared to visible light in these vdW heterostructures can be achieved. Appropriate valence and conduction band edges with standard redox potentials provide enough force to drive the photogenerated electrons and holes to dissociate water into H^+/H_2 and O_2/H_2O, thus making MSSe-g-GaN (M = Mo, W) vdW heterostructure promising for photocatalytic water splitting at pH = 0, while MoSSe-g-GaN in model-II fails to reduce water at pH = 7.

Physical Chemistry Chemical Physics Accepted Manuscript

This journal is © The Royal Society of Chemistry [year]

View Article Online
DOI: 10.1039/D0CP03434G

Published on 21 August 2020. Downloaded by University of Vermont on 8/23/2020 5:51:36 PM.

Physical Chemistry Chemical Physics Accepted Manuscript

Acknowledgement

Higher Education Commission of Pakistan (Grant No.5727/KPK/NRPU/R&D/HEC2016) and Vietnam National Foundation for Science and Technology Development (NAFOSTED) under grant number 103.01-2019.05 are gratefully acknowledged.

References

1 A.-Y. Lu, H. Zhu, J. Xiao, C.-P. Chuu, Y. Han, M.-H. Chiu, C.-C. Cheng, C.-W. Yang, K.-H. Wei, Y. Yang *et al.*, *Nat. Nanotechnol.*, 2017, **12**, 744–749.

2 J. Zhang, S. Jia, I. Kholmanov, L. Dong, D. Er, W. Chen, H. Guo, Z. Jin, V. B. Shenoy, L. Shi *et al.*, *ACS Nano*, 2017, **11**, 8192–8198.

3 T. Hu, F. Jia, G. Zhao, J. Wu, A. Stroppa and W. Ren, *Phys. Rev. B*, 2018, **97**, 235404.

4 C. Xia, W. Xiong, J. Du, T. Wang, Y. Peng and J. Li, *Phys. Rev. B*, 2018, **98**, 165424.

5 Y. Luo, S. Wang, K. Ren, J.-P. Chou, J. Yu, Z. Sun and M. Sun, *Phys. Chem. Chem. Phys.*, 2019, **21**, 1791–1796.

6 K. Ren, M. Sun, Y. Luo, S. Wang, J. Yu and W. Tang, *Appl. Surf. Sci.*, 2019, **476**, 70–75.

7 L.-Y. Gan, Q. Zhang, Y. Cheng and U. SchwingenschloÌĹgl, *J. Phys. Chem. Lett.*, 2014, **5**, 1445–1449.

8 T. Roy, M. Tosun, X. Cao, H. Fang, D.-H. Lien, P. Zhao, Y.-Z. Chen, Y.-L. Chueh, J. Guo and A. Javey, *ACS Nano*, 2015, **9**, 2071–2079.

9 O. Lopez-Sanchez, E. Alarcon Llado, V. Koman, A. Fontcuberta i Morral, A. Radenovic and A. Kis, *ACS Nano*, 2014, **8**, 3042–3048.

10 Z. Yu, Y. Pan, Y. Shen, Z. Wang, Z.-Y. Ong, T. Xu, R. Xin, L. Pan, B. Wang, L. Sun *et al.*, *Nat. Commun.*, 2014, **5**, 1–7.

11 X. Hong, J. Kim, S.-F. Shi, Y. Zhang, C. Jin, Y. Sun, S. Tongay, J. Wu, Y. Zhang and F. Wang, *Nat. Nanotechnol.*, 2014, **9**, 682–686.

12 R. Bose, G. Manna, S. Jana and N. Pradhan, *Chem. Commun.*, 2014, **50**, 3074–3077.

13 B. Amin, N. Singh and U. Schwingenschlögl, *Phys. Rev.w B*, 2015, **92**, 075439.

14 Z. Guan, C.-S. Lian, S. Hu, S. Ni, J. Li and W. Duan, *J. Phys. Chem. C*, 2017, **121**, 3654–3660.

15 M. Idrees, H. Din, R. Ali, G. Rehman, T. Hussain, C. Nguyen, I. Ahmad and B. Amin, *Phys. Chem. Chem. Phys.*, 2019, **21**, 18612–18621.

16 H. Din, M. Idrees, A. Albar, M. Shafiq, I. Ahmad, C. V. Nguyen and B. Amin, *Phys. Rev.B*, 2019, **100**, 165425.

17 Z. Y. Al Balushi, K. Wang, R. K. Ghosh, R. A. Vilá, S. M. Eichfeld, J. D. Caldwell, X. Qin, Y.-C. Lin, P. A. DeSario, G. Stone *et al.*, *Nat. Mater.*, 2016, **15**, 1166–1171.

18 M. Sun, J.-P. Chou, Q. Ren, Y. Zhao, J. Yu and W. Tang, *Appl. Phys. Lett.*, 2017, **110**, 173105.

19 A. Onen, D. Kecik, E. Durgun and S. Ciraci, *Phys. Rev. B*, 2016, **93**, 085431.

20 H. Shu, X. Niu, X. Ding and Y. Wang, *Appl. Surf. Sci.e*, 2019, **479**, 475–481.

21 M. Sun, J.-P. Chou, J. Yu and W. Tang, *Phys. Chem. Chem. Phys.*, 2017, **19**, 17324–17330.

22 J. Wang, H. Shu, P. Liang, N. Wang, D. Cao and X. Chen, *J. Phys. Chem. C*, 2019, **123**, 3861–3867.

23 P. Lou and J. Y. Lee, *ACS Appl. Mater. Interfaces*, 2020, **12**, 14289–14297.

24 W. Kohn and L. J. Sham, *Phys. Rev.*, 1965, **140**, A1133.

25 G. Kresse and J. Furthmüller, *Phys. Rev. B*, 1996, **54**, 11169.

26 S. Grimme, *J. Comput. Chem.*, 2006, **27**, 1787–1799.

27 J. P. Perdew, K. Burke and M. Ernzerhof, *Phys. Rev. Lett.*, 1996, **77**, 3865.

28 J. Heyd, G. E. Scuseria and M. Ernzerhof, *J. Chem. Phys.*, 2003, **118**, 8207–8215.

29 J. D. Gale, *J. Chem. Soc., Faraday Trans.*, 1997, **93**, 629–637.

30 J. D. Gale and A. L. Rohl, *Mol. Simul.*, 2003, **29**, 291–341.

31 Z. Cui, K. Ren, Y. Zhao, X. Wang, H. Shu, J. Yu, W. Tang and M. Sun, *Appl. Surf. Sci.*, 2019, **492**, 513–519.

32 S. Wang, C. Ren, H. Tian, J. Yu and M. Sun, *Phys. Chem. Chem.l Phys.*, 2018, **20**, 13394–13399.

33 S. Wang, H. Tian, C. Ren, J. Yu and M. Sun, *Sci. Rep.*, 2018, **8**, 1–6.

34 M. Yagmurcukardes, C. Sevik and F. Peeters, *Phys. Rev. B*, 2019, **100**, 045415.

35 S.-S. Ding, W.-Q. Huang, Y.-C. Yang, B.-X. Zhou, W.-Y. Hu, M.-Q. Long, P. Peng and G.-F. Huang, *J. Appl. Phys.*, 2016, **119**, 205704.

36 Y. Si, H.-Y. Wu, J.-C. Lian, W.-Q. Huang, W.-Y. Hu and G.-F. Huang, *Phys. Chem. Chem. Phys.*, 2020, **22**, 3037–3047.

37 Y. Li, Y.-L. Li, B. Sa and R. Ahuja, *Catal. Sci. Tech.*, 2017, **7**, 545–559.

38 V. D. S. Ganesan, J. Linghu, C. Zhang, Y. P. Feng and L. Shen, *Appl. Phys. Lett.*, 2016, **108**, 122105.

39 J. Liao, B. Sa, J. Zhou, R. Ahuja and Z. Sun, *J. Phys. Chem. C*, 2014, **118**, 17594–17599.

40 G. Henkelman, A. Arnaldsson and H. Jónsson, *Computat. Mater. Sci.*, 2006, **36**, 354–360.

41 D. D. Vo, T. V. Vu, T. H. T. Nguyen, N. N. Hieu, H. V. Phuc, N. T. Binh, M. Idrees, B. Amin and C. V. Nguyen, *RSC Adv.*, 2020, **10**, 9824–9832.

42 B.-J. Wang, X.-H. Li, R. Zhao, X.-L. Cai, W.-Y. Yu, W.-B. Li, Z.-S. Liu, L.-W. Zhang and S.-H. Ke, *J. Mater. Chem. A*, 2018, **6**, 8923–8929.

43 F. Opoku, K. K. Govender, C. G. C. E. van Sittert and P. P. Govender, *New J. Chem.*, 2017, **41**, 8140–8155.

44 X. Peng, F. Tang and A. Copple, *J. Phys. Condens. Matter*, 2012, **24**, 075501.

45 K. M. Alam, P. Kumar, P. Kar, U. K. Thakur, S. Zeng, K. Cui and K. Shankar, *Nanoscale Adv.*, 2019, **1**, 1460–1471.

46 Z. Cui, X. Wang, E. Li, Y. Ding, C. Sun and M. Sun, *Nanoscale Res. Lett*, 2018, **13**, 1–9.

47 A. Togo, F. Oba and I. Tanaka, *Phys. Rev. B*, 2008, **78**, 134106.

48 C. Gong, H. Zhang, W. Wang, L. Colombo, R. M. Wallace and

View Article Online
DOI: 10.1039/D0CP03434G

K. Cho, *Appl. Phys. Lett.*, 2013, **103**, 053513.

49 J. Kang, S. Tongay, J. Zhou, J. Li and J. Wu, *Appl. Phys. Lett.*, 2013, **102**, 012111.

50 H.-P. Komsa and A. V. Krasheninnikov, *Phys. Rev. B*, 2013, **88**, 085318.

51 K. Kośmider and J. Fernández-Rossier, *Phys. Rev. B*, 2013, **87**, 075451.

52 L. Britnell, R. Ribeiro, A. Eckmann, R. Jalil, B. Belle, A. Mishchenko, Y.-J. Kim, R. Gorbachev, T. Georgiou, S. Morozov *et al.*, *Science*, 2013, **340**, 1311–1314.

53 W. J. Yu, Y. Liu, H. Zhou, A. Yin, Z. Li, Y. Huang and X. Duan, *Nat. Nanotechnol.*, 2013, **8**, 952–958.

54 O. Lopez-Sanchez, D. Lembke, M. Kayci, A. Radenovic and A. Kis, *Nat. Nanotechnol.*, 2013, **8**, 497–501.

55 J. Liu, X. Fu, S. Chen and Y. Zhu, *Appl. Phys. Lett.*, 2011, **99**, 191903.

56 H. L. Zhuang and R. G. Hennig, *Phys. Rev. B*, 2013, **88**, 115314.

57 J. M. Bolts and M. S. Wrighton, *J. Phys. Chem.*, 1976, **80**, 2641–2645.

58 T. A. Pham, D. Lee, E. Schwegler and G. Galli, *J. Am. Chem. Soc.*, 2014, **136**, 17071–17077.

59 X. Li, J. Yu, J. Low, Y. Fang, J. Xiao and X. Chen, *J. Mater. Chem. A*, 2015, **3**, 2485–2534.

Published on 21 August 2020. Downloaded by University of Vermont on 8/23/2020 5:51:36 PM.

Physical Chemistry Chemical Physics Accepted Manuscript

This journal is © The Royal Society of Chemistry [year]